

Christoph Brandes, Armelle Cathy Megne Tague, Stephen Kroll, Laura Treccani, Kurosch Rezwan



Gel casting of large area micro- and sub-micropatterned thin ceramic tapes

Journal Article as: peer-reviewed accepted version (Postprint)

DOI of this document* (secondary publication): 10.26092/elib/2602

Publication date of this document: 20/10/2023

* for better findability or for reliable citation

Recommended Citation (primary publication/Version of Record) incl. DOI:

Christoph Brandes, Armelle Cathy Megne Tague, Stephen Kroll, Laura Treccani, Kurosch Rezwan,
Gel casting of large area micro- and sub-micropatterned thin ceramic tapes,
Ceramics International, Volume 42, Issue 4, 2016, Pages 5036-5044, ISSN 0272-8842,
<https://doi.org/10.1016/j.ceramint.2015.12.015>

Please note that the version of this document may differ from the final published version (Version of Record/primary publication) in terms of copy-editing, pagination, publication date and DOI. Please cite the version that you actually used. Before citing, you are also advised to check the publisher's website for any subsequent corrections or retractions (see also <https://retractionwatch.com/>).

This document is made available under a Creative Commons licence.

The license information is available online: <https://creativecommons.org/licenses/by-nc-nd/4.0/>

Take down policy

If you believe that this document or any material on this site infringes copyright, please contact publizieren@suub.uni-bremen.de with full details and we will remove access to the material.

Gel casting of large area micro- and sub-micropatterned thin ceramic tapes

Christoph Brandes^a, Armelle Cathy Megne Tague^a, Stephen Kroll^{a,b}, Laura Treccani^{a,*},
Kurosch Rezwani^{a,b}

^aAdvanced Ceramics, University of Bremen, Am Biologischen Garten 2, 28359 Bremen, Germany

^bMAPEX – Centre for Materials and Processes, University of Bremen, 28359 Bremen, Germany

Abstract

In this study an easy-to-use ceramic processing technique based on temperature-controlled ionotropic gelation of alginate is presented. This method is the breakthrough for simultaneously large scale tape casting and high quality patterning of thin ceramic tapes. Alumina powder ($d_{50} = 205$ nm) is used to cast flexible and on demand shapeable tapes. Compared to conventional ceramic micropatterning, ionotropic gelation combines complexity of the patterned structure over large-scale areas, a high pattern resolution down to sub- μ m regime (~ 400 nm) and tape thickness below 300 μ m. Obtained green and sintered (1350 °C) micro- and sub-micropatterns are characterized by SEM and quantitative 3D-profilometry focusing on both, pattern quality and pattern aspect ratio. The results show that reproducible thin ceramic tapes featuring positive and negative patterns maintain their aspect ratios after demolding, drying and sintering. This processing route represents a versatile tool for designing tailored ceramics for e.g. microelectromechanical engineered systems, biomaterial or microfluidic applications.

Keywords: Gel casting; Flexible ceramic tape; Micropatterning; High-precision pattern-contour; 3D-surface profilometry.

1. Introduction

Engineering ceramic surfaces with specific topographies, defined geometries and controllable structural features are of particular relevance for engineering, biotechnological, biomedical and environmental applications. Surface structures can be beneficially used for increasing and widening the material properties such as bioactivity [1,2], crack resistance and mechanical strength [3,4]. Physical surface modification is based on tailoring the topographic properties such as the surface roughness or the structural pattern. Surface structures ranging from 100 nm to 1000 nm can interact for example with electromagnetic waves [5,6] and are relevant for laser applications and/ or optical security systems like holograms [7]. Ceramic surface patterns with sizes from 1 μ m to 10 μ m can be used to guide cell growth [8], prevent bacterial adhesion [9] and growth, or to influence flow resistance [10], as well as flow

characteristics [11]. In addition to their outstanding high thermal [12], chemical [13] and mechanical resistance [14], some ceramic materials like yttrium aluminum garnet, alumina, zirconia and calcium phosphates feature additional attractive properties like photoluminescence [15], abrasion resistance [16], and bioactivity [17–19], respectively.

Due to the chemical inertness, high hardness and brittleness of ceramic materials such as alumina (Al_2O_3) and zirconia (ZrO_2), patterning techniques based on micro milling [20], micro grinding [21], laser or electron patterning [22,23] or chemical etching [24] are hardly suitable. These methods can be applied on sintered materials and they enable structures with limited heights, small patterned areas, low resolution and topographies with high roughness. In contrast, micromolding [25] as well as embossing [8] are patterning methods, which give higher quality structures. They are applied before sintering, during shaping and preparation of the green bodies or tapes.

Micromolding techniques use elastomeric material, like polydimethylsiloxane (PDMS), as patterned form. It allows the successful fabrication of small-scaled sample sizes in the

lower cm-regime with patterns down to the μm -scale [26]. Chen et al. used a modified micromolding process to create ZnO green bodies with sub-micrometer pillars (200–700 nm) [25]. However, the influence of particle size and sintering on the pattern resolution, or the patterning of more complex shapes was not further considered. The main disadvantage of the micromolding technique is related to the required gravity-driven sedimentation of the suspension which makes a defect-free demolding without shape deformation challenging. This holds especially for usually prepared binder-free, stiff green bodies. The difficulty of demolding increases for increasing shape complexity and object sizes if the particle interactions cannot be adjusted to permit unwanted demolding and cracks [27].

Compared to micromolding techniques the embossing process uses ceramic green tapes with high binder and plasticizer content (> 20 wt%) to ensure shape retention. Embossing can be used for flexible ceramic sheets, which show a high aspect ratio pattern. In most cases, a metal stamp is pressed with precise force control into the substrate tape to obtain the target structure. Due to shifting of the ceramic mass by pressing, generation of large patterned areas is limited. Especially sharp edges with high contour accuracy are not possible to produce [28].

In this study we present an easy-to-use ceramic processing technique for tailored micro- and sub-micropatterning of thin ceramic tapes, which is based on a temperature-controlled ionotropic gelation of alginate. This method combines the advantages of both, micromolding and embossing (i.e. large scale tape area, high pattern resolution, different pattern sizes, low binder content). The here described patterning method allows simultaneously large scale casting and micro- and sub-micropatterning of flexible ceramic tapes. The ceramic processing bases on ionotropic gelation of an alginate containing alumina slurry with calcium iodate as temperature triggered cross linker, a production technique that has been successfully used for rigid solids [29] and ceramic membranes [30]. We show that with this straightforward processing route a large scale patterning (dm-range) can be easily mastered and that structure limitations are only given by the used initial alumina particle size. This pattern technique allows the preparation of flat surfaces as well as curved structures being the ideal choice for several ceramic applications.

2. Experimental procedure

2.1. Materials

α -Alumina powder (Al_2O_3 , TM-DAR, Taimei Chemicals, Japan, $d_{50}=205$ nm, specific surface area 14.8 m²/g, Lot.: 9105, purity 99.99%) was purchased from Krahn, Germany. α -Alumina sintering bed was provided by Almatix, Germany (CL 5000, specific surface area 0.20 – 0.35 m²/g, crystal size 3.1 – 5.1 μm , Lot.: 1414497261). Ammonium hydroxide (NH_4OH , Product No: 30501, Lot.: SZBB0250), calcium iodate ($\text{Ca}(\text{IO}_3)_2$, Product No: 30501, Lot.: MKBC8376V) and alginic sodium salt from brown algae (alginate medium viscosity,

Product No.: 2033, Lot.: 051M0054V) were obtained from Sigma-Aldrich Chemie GmbH, Germany. Protanal LFR 5/60 sodium alginate (Lot.: H10673, FMC Biopolymer USA), triammonium citrate (TCA, Product No: AB110464, Lot.: 1228037, abcr GmbH, Germany), polytetrafluoroethylene-foil (PTFE, thickness 0.05 – 1 mm, Hightechflon GbR, Germany) and polydimethylsiloxane (PDMS, Sylgard® 184, Lot.: 0007280543, Dow Corning Corporation, MIDLAND MI, USA) were purchased from different suppliers as indicated. Double deionized water (ddH_2O) with an electrical resistance of 18 M Ω (Synergy®, Millipore, Germany) was used for all experiments.

2.2. Characterization of alumina particles

The particle size and particle size distribution of Al_2O_3 particles were measured via dynamic light scattering (DLS) using a Malvern Zetasizer ZSP (Worcestershire, UK). Al_2O_3 particles were suspended in ddH_2O and sonicated with an ultrasound horn (Sonifier 450, Branson; output: 150 pulse rate 0.5 s) for 15 min to break agglomerates. For each measurement the suspension was diluted according to the manufacturer's recommendation until the polydispersity index was stable and below 0.3.

Scanning electron microscopy (SEM) of the Al_2O_3 particles was carried out at 10 kV and without any conductive coating (Supra 40, Carl Zeiss, Field emission, Germany).

2.3. Fabrication of micropatterned ceramic tapes

The processing route for the fabrication of patterned ceramic tapes is schematically shown in Fig. 1A. All processing steps including slurry preparation (1), patterning with polymer-foil (2), slurry gelation (3), demolding (4), drying (5) and sintering (6) are described. Detailed information about each processing step is given in the following sections.

2.4. Alumina slurry preparation

The ceramic slurry was prepared using a process adapted from Brandes et al. [30]. 0.6 g of each alginate (gel-former) were dissolved in 50 mL ddH_2O (solvent) at room temperature (RT) and mixed for 30 min at 300 rpm (IKA Rw20.n, Staufen, Germany). After complete dissolution of the alginate, the pH was adjusted to pH 9 using NH_4OH to ensure optimum solution viscosity. TCA (0.6 wt%) was used as dispersant to stabilize Al_2O_3 particles [31]. Afterwards 180 g Al_2O_3 (ceramic matrix) was slowly added to the alginate solution under continuous stirring for 1.5 h at 1900 rpm at RT for obtaining agglomerate-free slurries. To reduce frictional heating and water evaporation, the slurry was kept in a cooling bath (~ 4 °C). Afterwards, the slurry (~ 48 vol% solid content) was cooled in a fridge until its temperature was below 10 °C. For cross-linking 2 g $\text{Ca}(\text{IO}_3)_2$ were added to the slurry. Without addition of $\text{Ca}(\text{IO}_3)_2$ the slurry can be stored for weeks at 4 °C, it remains stable, and patterned ceramic tapes from the same batch can be fabricated on different working days.

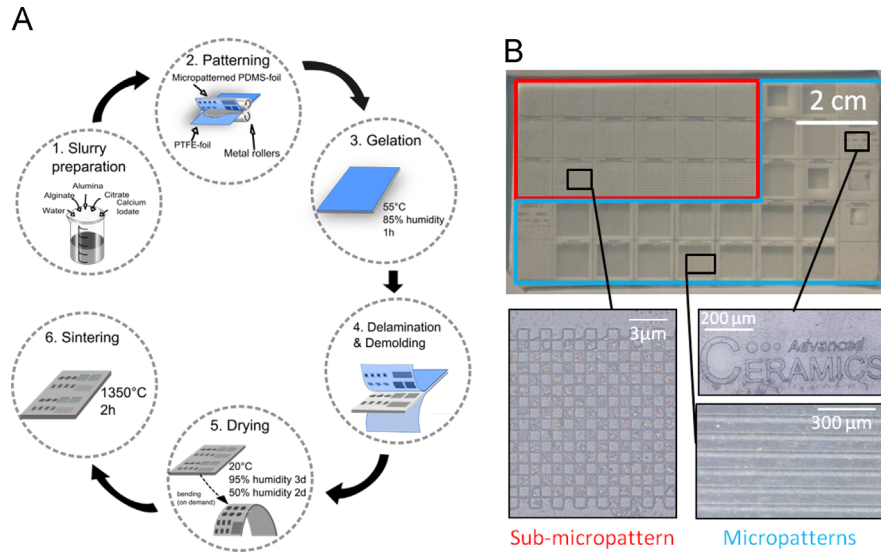


Fig. 1. (A) Schematic overview of the processing route for (sub-) micropatterned alumina tapes describing all processing steps. (B) Photograph of a PDMS-foil used as template with different micro- and sub-microstructures and patterns. In the insets representative micro- and sub-micropatterns are shown. The PDMS-foils were prepared according to the method described by Holthaus et al. [26].

2.5. Patterning and gelation

As shown Fig. 1A (step 2), the Al_2O_3 slurry was spread with the help of two metal rollers between a patterned PDMS-foil (Fig. 1B) and a PTFE-foil used as support and backside for structuring. The PTFE-foil, ceramic slurry and micropatterned PDMS-foil were stacked and rolled between two metal rollers. The thickness of the ceramic tapes can be freely varied by adjusting the distance between the metal rollers and by taking into account the thickness of the PDMS- and PTFE-foils. Typical thickness of PDMS and PTFE foils are ~ 1 mm and 0.25 mm, respectively.

To ensure homogeneous slurry spreading, PDMS structure filling and a uniform ceramic tape thickness the stack was rolled five times. Then, the stack was stored for 1 h in a climate control chamber (KBF, Binder, Tuttlingen, Germany) at constant conditions. The temperature was set at 55 °C to increase $\text{Ca}(\text{IO}_3)_2$ solubility and release of Ca^{2+} -ions which initiate the gelation process (Fig. 1A, step 3). The relative humidity (RH) was set at 85% in order to prevent drying and possible crack formation during gelling and green body consolidation.

2.6. Delamination, drying and sintering

After gelation and consolidation, the PTFE- and PDMS-foils were carefully pulled off and the micropatterned ceramic green tape was removed by delamination (Fig. 1A, step 4). The gelled and not dried patterned tape is still flexible and bendable. It can be freely shaped into customizable, complex geometries. Afterwards, the micropatterned ceramic green tape was dried in a climate control chamber (see Fig. 1A, step 5) at 95% RH for 3 days and at 50% RH for 2 additional days. The temperature was kept constant at 20 °C. At these conditions the

formation of defects and uncontrolled wrinkling of the gelled tape can be avoided. The tapes were sintered (Fig. 1A, step 6) at 1350 °C for 2 h with heating and cooling rates of 300 K/h and 500 K/h, respectively (HT 08/17, Nabertherm, Germany). Due to the low amount of organic components (< 2.5 wt%) a debinding step during the heating was not necessary. For a homogenous heat distribution all samples were sintered inside a sinter bed consisting of α -alumina (CL 5000). A sintering temperature of 1350 °C and a dwell time of 2 h were selected to obtain dense tapes. The unusual low sintering temperature for alumina is in accordance with the supplier's recommendations and based on the small size of the powder and its high specific surface.

2.7. Characterization of patterned green and sintered ceramic tapes

The thickness of the ceramics tapes was measured before and after sintering using an optical microscope (Keyence VHX-600 Digital Microscopy, Frankfurt, Germany). Each measurement was repeated five times at different tape positions for statistical significance. The open and total porosity were determined via Archimedes method. Prior to measurement the samples were dried at 70 °C. The density of the Al_2O_3 -particles was measured with a He-Pycnometer (Pycnomatic ATC, Porotec) in order to calculate the total porosity.

The patterned ceramic surfaces were imaged by SEM at 10 kV without conductive coating (Supra 40, Zeiss, Field emission, Germany).

Surface roughness and pattern height, width and length and different aspect ratios (height/ width, length/ width) were determined by contactless 3-D profilometry (PIμ 2300, Sensorfar technology, Terrassa, Spain). Magnifications of 210-fold for micropatterns and 3150-fold for sub-micropatterns were

used. The aspect ratio values of five identical patterns were used to calculate the average values and the standard deviations and for statistical significance. The surface roughness (Ra) was measured according to ISO 4287 [32] and non-patterned ceramic tapes fabricated as previously described served as reference.

3. Results

3.1. Al_2O_3 particle characterization

The size and morphology of the Al_2O_3 particles used for fabricating gel-casted patterned tapes are given in Fig. S1A. The Al_2O_3 particles are irregularly shaped and non-spherical. The by DLS measurements obtained particle size distribution ranged from 80 to 350 nm and the average particle size (d_{50}) is 205 nm (Fig. S1B).

3.2. Tape characterization

Green tapes with wide thickness ranging from 300 μm to 10 mm could be easily obtained using the same procedure as described in Fig. 1A. The thickness of the tapes was determined after drying and the thinnest green tape obtainable has a thickness of $372 \pm 5 \mu\text{m}$ after drying. Thicker tapes with thicknesses up to 10 mm were also obtained but in this study only the thinnest tapes are considered.

Gelled and not dried ceramic tapes had a high flexibility and could be easily bended or twisted in the desired shape (Fig. 2A). In general, thicker tapes are easier to handle. In order to fabricate curved tapes, porous polymer polyurethane (PU) foams were used as support. Thereby the shape and stability of the tapes during gelling and drying was maintained. A curved thin ceramic tape after sintering is exemplarily shown in Fig. 2B.

Defects like tear offs or bubbles caused by shaping (e.g. bending of the gelled tape) were not observed via SEM and the profilometer analyses.

In Fig. 2C the edge of a tape and in Fig. 2D1 and D2 SEM micrographs of representative rectangular and circular micropatterns are shown.

Sufficient mechanical stability for sample handling was obtained using a sintering temperature of 1350 $^{\circ}\text{C}$ and a dwell time of 2 h. After sintering an isotropic shrinkage of $\sim 22\%$ was determined. For instance, after sintering dried green tapes with thickness of $372 \pm 5 \mu\text{m}$ shrunk to $291 \pm 5 \mu\text{m}$ (Fig. 2C). The density of the sintered tape was around 95%.

The surface roughness for green tapes was $142 \pm 28 \text{ nm}$ and for sintered tapes $113 \pm 24 \text{ nm}$, respectively. The patterned PDMS-foil surface roughness $< 18 \text{ nm}$ was determined.

3.3. Surface pattern characterization

Ceramic patterns in the micrometer ($> 1 \mu\text{m}$) and sub-micrometer ($< 1 \mu\text{m}$) range were obtained. Pattern size depended on the pattern of the PDMS-foil used as template (Fig. 1B).

In this study the topological features of two different types of model patterns were characterized: complex shaped micropattern with the “Advanced Ceramics” logo and a sub-micrometer pattern with a regular pillar-like structure.

The first pattern type (logo) letters with curves, edges and heights of 25 μm is used to assess the accuracy in the lower μm range of the presented gel-casting method.

The second pattern type consists of regularly arrangement pillars with heights in the sub-micrometer range ($\sim 500 \text{ nm}$ and diameter of $\sim 4 \mu\text{m}$). In addition the resolution limits in sub-micropatterning was tested by creating both positive and negative patterns using the logo structure. A positive pattern structure is defined as a ceramic pattern at which the actual pattern is standing out of the surface, and consequently the topological structure is protruded from the surface. The

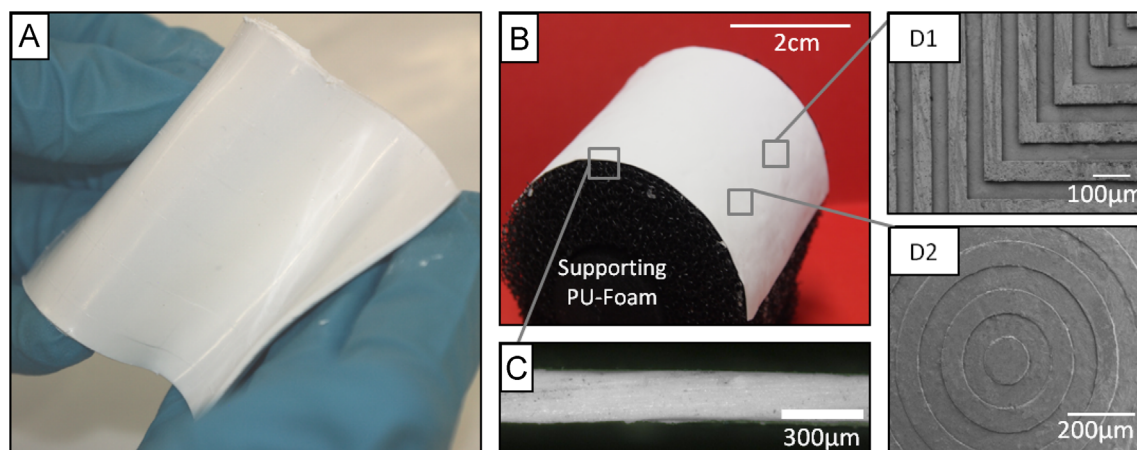


Fig. 2. (A) A photograph of a demolded gelled and therefore flexible ceramic tape. (B) Photograph of a bended alumina tape sintered at 1350 $^{\circ}\text{C}$ for 2 h gelled and dried on a polyurethane (PU) foam used as support. (C) A light microscopic image of the tape thickness. (D) Representative SEM micrographs of rectangular (D1) and circular (D2) surface micropatterns.

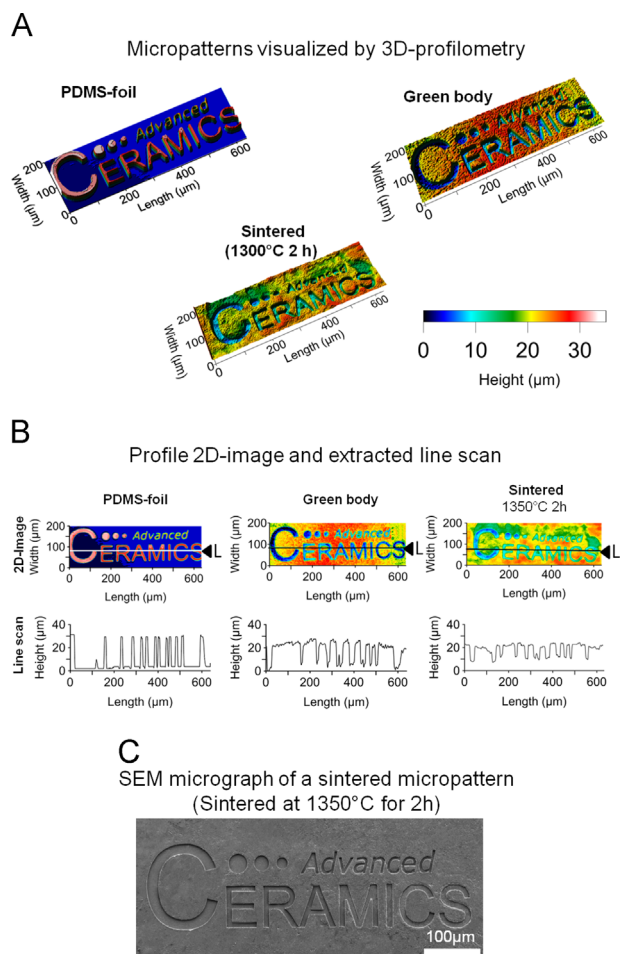


Fig. 3. Visualization of the micropatterned PDMS-foil and ceramic micro-patterned tapes in the green and sintered state. (A) 3D-profilometer images, (B) Compressed 2D-images and extracted line profile scans of PDMS molds and micropatterns after drying (green body) and sintering. (C) SEM micrograph of the sintered “Advanced Ceramics” logo. (For interpretation of the references to color in this figure legend, the reader is referred to the web version of this article.)

Table 1
Micropattern dimensions and shrinkages of the complex shaped logo “Advanced Ceramics” and a selected logo letter (“i” as representative) in relation to used initial PDMS mold, and obtained green body and sintered ceramic.

	PDMS-foil	Green body	Sintered sample (1350 °C for 2 h)
Logo- Pattern dimensions and obtained shrinkage values			
Logo length			
μm	643.8 ± 1.0	629.3 ± 0.5	557.3 ± 1.7
Shrinkage (%)		$2\% \pm 0.1\%$	$13\% \pm 0.3\%$
Logo width			
μm	175.2 ± 0.7	162.5 ± 1.6	148.3 ± 1.6
Shrinkage (%)		$7\% \pm 1\%$	$15\% \pm 1\%$
Aspect ratio			
Logo (width/ length)	0.27	0.26	0.27
Letter dimensions and obtained shrinkage values			
Letter height			
(μm)	17.8 ± 0.3	17.4 ± 0.5	15.8 ± 0.7
Shrinkage (%)		$2\% \pm 3\%$	$11\% \pm 4\%$
Letter width			
(μm)	12.8 ± 0.7	12.2 ± 0.7	11.2 ± 0.5
Shrinkage (%)		$5\% \pm 6\%$	$13\% \pm 4\%$
Aspect ratio			
Letter (height /width)	1.39	1.42	1.41

opposite is defined as negative patterning, at which the pattern surface is below the main surface level.

3.3.1. Characterization of micropatterned ceramic surfaces

To determine the micropattern structure as well as changes during the manufacturing process of the PDMS-foil, 3D-imaging profilometry of green and sintered tape surfaces was applied. Furthermore the 3D-images were applied to identify any potential pattern defects (e.g. tear offs or bubbles). The PDMS-foil, the ceramic green tape and the sintered tape with the “Advanced Ceramics” logo are shown in Fig. 3A.

After the gelling and drying step, the green tapes can be easily detached from the PDMS-foil and after sintering defect-free patterns and logo letters were obtained.

Structure shrinkage after drying and after sintering was observed as previously described (see Section 3.2). Line scans extracted from 3D-profilometry enable the analysis of pattern accuracy and the shrinkage during drying and sintering (Fig. 3B). The lines in the images which are created from the compressed 3D-profilometry measurements show the positions used to generate the extracted line scan. Based on the values the determination of the pattern aspect ratios is possible and the micropattern accuracy of the green and sintered parts can be evaluated.

The sizes, and size changes from initial PDMS-pattern to green and sintered tape as well as aspect ratios of the logo and of a selected, representative letter (“i”) are summarized in Table 1. After drying shrinkage of 2–7% was determined for both the logo structure and the selected logo letters. An additional shrinkage of 13–15% (logo) and 11–13% (individual letters) was observed after sintering.

No changes of the aspect ratios for the logo structure (ratio between width and length) as well as for the individual letter (ratio between height and width) were determined during the individual processing steps. This indicates that ceramic micropatterns with high contour accuracy are obtained after drying

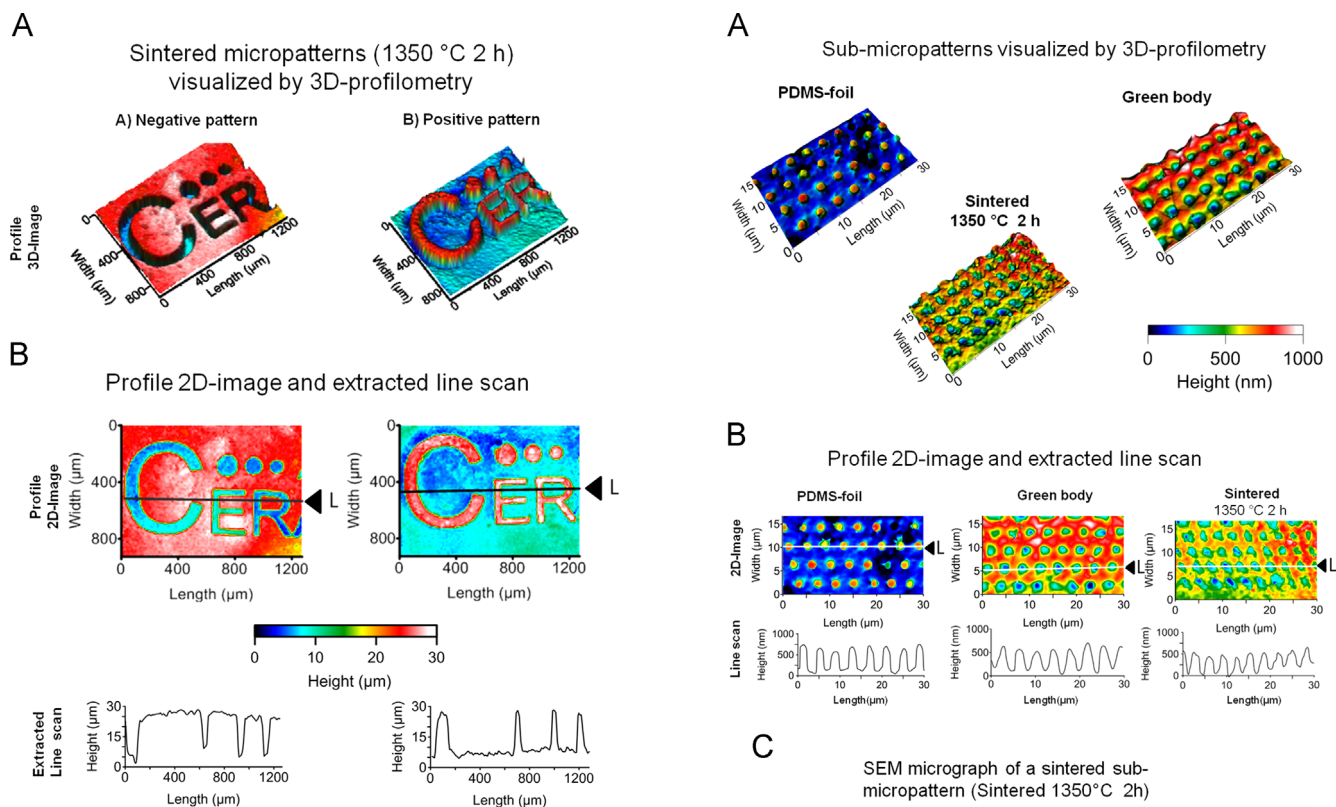


Fig. 4. Comparison of negative (A) and positive (B) logo micropatterns visualized by 3D profilometry.

and sintering. Despite the sample shrinkage the readability of the micropatterned logo “Advanced Ceramics” is still given after sintering as shown by the SEM micrograph of a sintered micropatterned surface (Fig. 3C).

3.3.2. Negative and positive micropatterning

To demonstrate the versatility of the developed patterning method based on gel casting, negative and positive imprints of the micropatterned logo “Advanced Ceramics” have been fabricated. Fig. 4 shows a section of three letters (“Cer”) of obtained 3D-profilometer images, the compressed 2D-images and the extracted line scans for sintered negative (A) and positive (B) micropatterns. Comparable surface topographies of the PDMS template height and depth (25 μm) are applied as well. Both negative and positive micropatterns, are successfully fabricated. As aspect ratios are unaltered during the whole process the opportunity to freely choose the surface topographic orientation for micropatterning is unlimited.

3.3.3. Characterization of regular sub-micropatterns

In accordance with the micrometer-scaled patterns (Figs. 3 and 4), 3D-profilometer measurements were used to analyze sub-micropatterns consisting of regularly arranged pillars with a height of ~ 500 nm and a diameter of ~ 4 μm . The surface topographies of the prepared sub-micropatterned PDMS-foil and the fabricated green and sintered tapes are presented in Fig. 5. The 3D-profilometer images (Fig. 5A) show the regular

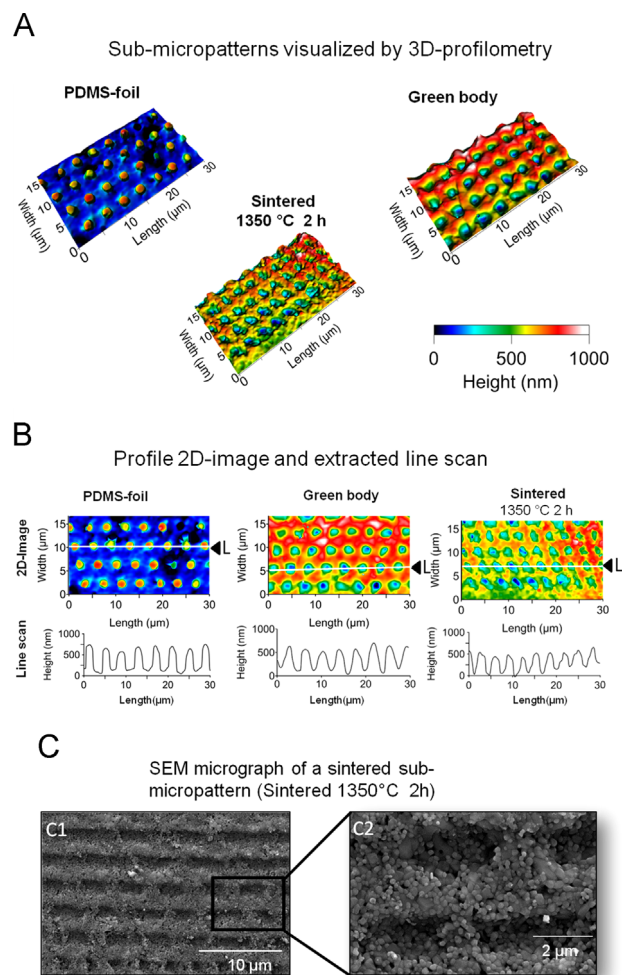
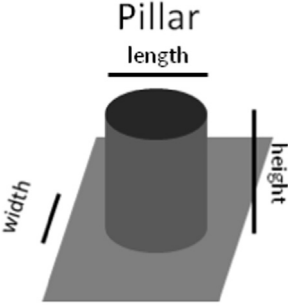
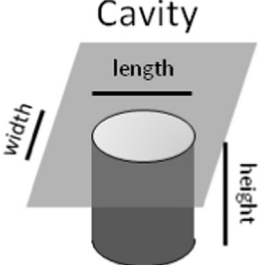


Fig. 5. 3D profilometer images (A) and compressed 2D-images as well as the extracted line scans (B) for sub-micropatterns show a regular pillar pattern of the PDMS-foil and obtained cavities for green and sintered patterns. C: SEM micrographs showing an overview (C1) and a detailed view (C2) of the sintered sub-micropatterned structure. (For interpretation of the references to color in this figure legend, the reader is referred to the web version of this article.)

arrangement of the pillar pattern on the PDMS-surface and cavities of the green body and the sintered surface.

The extracted line scans (exact position see Fig. 5B) and thereof the evaluated data for the sub-micropattern dimensions and shrinkage values (Table 2) show that single pillars of the PDMS-foil have a height of 498 ± 15 nm and a diameter of 3.7 ± 0.2 μm . The negative patterned green tape reveals cavity depths of 455 ± 73 nm and corresponds to isotropic drying shrinkage of 8.6%. The aspect ratio of the sub-micropattern was not influenced after gelling and drying. After sintering the cavity depth shrank of 15% with respect to the PDMS-foil, and the cavity final depth was 422 ± 30 nm. As shown by SEM micrographs in Fig. 5 (part C1), uniform cavity-like structures are obtained after sintering. Furthermore at higher magnification (Fig. 5, part C2) individual Al_2O_3 particles ($d_{50} = 205$ nm, Fig. S1B) can be identified. The numbers of particles counted in each cavity are typically two or three in height, and 12 ± 2 particles in the cavity length, which correspond to ~ 400 – 600 nm and ~ 2.4 – 2.8 μm , respectively.

Table 2
 Pattern shrinkage and changes of the aspect ratio during the process of manufacturing of sub-micropatterns.

Sub-micropattern dimensions and shrinkage values	PDMS-Mold Pillar dimension	Green Body Cavity dimension	Sintered 1350 °C 2 h Cavity dimension	
 <p>Pillar</p> <p>length</p> <p>width</p> <p>height</p>	Height			
	nm	498 ± 15	455 ± 73	422 ± 30
	Shrinkage		8.6% ± 6%	15% ± 7%
	Width			
	µm	3.7 ± 0.2	3.5 ± 0.3	2.9 ± 0.1
	Shrinkage		5% ± 8.6%	22% ± 3%
	Length			
	µm	4.0 ± 0.2	3.8 ± 0.2	3.1 ± 0.2
	Shrinkage		5% ± 5.3%	22% ± 6%
	Aspect ratio			
Ratio of height/width	0.13	0.13	0.14	
Ratio of width/ length	0.93	0.92	0.94	
 <p>Cavity</p> <p>length</p> <p>width</p> <p>height</p>				

4. Discussion

4.1. Tape casting

The straightforward process of ionotropic gelation is beneficially used to create easily flexible micro- and sub-micropatterned oxide ceramic tapes. The method enables the fabrication of defect-free and uniform thin tapes (< 400 µm). Compared to conventional casted alumina ceramic tapes (25–80 wt% ceramics) with plasticizers [33] the solid loading (~80 wt%) is one of the highest. An alternative tape casting process, based on alginate containing-slurries with the same amount of alginate (< 2 wt%) and ceramic powder, uses the direct gelation technique [34,35]. Hereby, a tape is obtained using a ceramic slurry, that is immersed into a cross-linking solution of Ca²⁺-ions. The ions diffuse into the tape and induce the gelation. Compared to ceramic green tapes made by a direct gelation technique [34], our presented method with Ca (IO₃)₂ shows no diffusion limitations and permits the fabrication of tapes of varying thicknesses. Additionally it allows the application of micropatterns. For both methods the obtainable minimal tape thickness is ~300 µm. The maximal tape thickness obtainable by direct gelation is limited by Ca²⁺ concentration and immersion time and/or contact surface.

The minimal tape thickness is the limitation for a proper handling of the green tapes and the handling difficulty increases with the decreased tape thickness. Compared to

established aqueous-based alumina tape casting methods our produced tapes are in the same order of magnitude for the thickness [36]. The production of thinner tapes (< 250 µm) might be possible by increasing the amount of alginate with a large ratio of α-L-gulonate blocks [37] or by increasing the cross-linker content [38]. But both strategies are accompanied by an increased viscosity and decreased handling time during the manufacturing process. Therefore these process variations can effect disadvantageously the homogeneous filling of the PDMS-foil (e.g. PDMS), resulting in insufficient micropattern qualities of the fabricated ceramic samples.

4.2. Pattern quality of micro- and sub-micropatterned ceramics

The most important advantage of the used ionotropic-gelation method for tape casting is the simultaneously large scale patterning of ceramics with different pattern sizes (micro- and sub-micro regime) and different pattern types including positive and negative patterns. The quality of the pattern and their topological profile is quantified by 3D-profilometry and two different pattern structures served as model structures with different possible application areas. Firstly, a logo (“Advanced Ceramics”) serves as a complex model structure which can be used for example as a security feature for industrial ceramic components. The pattern dimensions are in a µm-scaled range (25–100 µm) and e.g. suitable for fluidic applications [39]. For

example Jagdeesh [40] showed, that patterns in this μm -range can be used to convert a hydrophilic Al_2O_3 surface into a super hydrophobic surface. The second applied pattern is based on the utilization of a template with stick out pillars in the sub-micrometer regime (~ 500 nm) and obtained cavities after patterning are interesting candidate e.g. for optical applications [41].

In the presented processing route both, the PDMS-foil as template and the gelled tape can be bent because of their elasticity and allows a defect-free demolding. Peeling off is additionally facilitated by the formation of a thin water layer on the surface of the casted gel which acts as lubricant. This behavior is a distinguishing mark from other patterning processes (e.g. embossing) where typically molds must be removed by combustion or harsh chemicals [42,43]. Furthermore the PDMS-foil is reusable several times (> 15) without an evident quality loss of the pattern structure.

Another benefit is related to the fact that the geometry type of pattern structure is not limited to preferred orientations. Pattern alignment has no influence on the final pattern quality. This includes that orientation of the pattern on the tape (i.e. negative or positive pattern) obtained by the manufacturing process is not important, nor the direction of demolding. Compared to conventional patterning techniques the produced pattern quality (edge accuracy, number of defects, topological surface details) is on the same level as soft-lithography [44] or stamp embossing [8]. Compared to continuous roller-based embossing methods the edges of the patterns produced via gel-casting are more precise [28]. Typically, embossing techniques are limited by the occurred mass shift in dependence of embossing pattern size [45]. This leads to the necessity of large differences in the pattern parameters (i.e. height, length and width of the pattern elements, as well as the distance of the single pattern elements). Otherwise the pattern and substrate can crack or fragment during sintering. Soft lithography often shows defect structures for positive patterns like rip offs [25,26] or micro-cracks [8]. Overall the results in our study show that the gel-casted micro- and sub-micropattern can be produced with high precision and reproducibility. Furthermore, the developed technique can be used for simultaneously positive and negative patterning being an advantage not given by the other patterning processes where typical procedures allow either one or the other pattern direction.

Another outstanding advantage of the gel-casting technique is the obtained resolution of the generated patterns, especially the sub-micropatterns. In the developed process the pattern height is only limited by the particle size of the used initial ceramic powder. In this study α -alumina particles with an average particle size (d_{50}) of 205 nm served as ceramic powder. Therefore the theoretical achievable lowest height is given by the particle diameter. In the case of single particle deposition the pattern height would be around 200 nm and our results show that after sintering the lowest feasible pattern height is 422 ± 30 nm which equals the height of two alumina particles and is very close to the theoretical assumptions. Even the deposition of single particle layers cannot be excluded. Due to the measurement resolution- and visualization limits of

the 3D-profilometer the preparation of such structures can be possible. The surface roughness of the green and sintered patterns is around half the size of the used alumina particles where the particle shape and their packing have also to be considered. The impact of the surface roughness on the pattern quality increases with decreasing pattern size. Especially, resulting blurring of pattern edges can be seen on the sub-micrometer patterns. While a regular patterning is still clearly visible, the plateau areas of the PDMS-foil profile get less clear copied to the ceramic surface. Better results can probably be achieved with smaller particles but high volume (~ 50 vol%) concentrations of nanoparticles are difficult to stabilize due to their high surface and the resulting surface interactions. Up to now, smaller pattern sizes have only been reported by Chen et al. [25] using 20 nm ZnO particles or by Nadum et al. [8] focusing on a similar pattern height but with a much larger pattern width. Due to the shrinkage behavior of the pattern structures significantly higher drying and sintering shrinkage rates are determined for the sub-micrometer patterns in comparison to the micrometer patterns. This result can be attributed to the effect that the number of ceramic particles involved in the pattern is much smaller compared to the overall structure. However, tension induced cracking by the different shrinkage rates between tape and the applied pattern has not been observed. It can be assumed that the ceramic particles in this small range have less contact during sintering and therefore, they can slightly move during sintering to relieve stress tensions.

5. Conclusion

This work shows that by ionotropic gelation, ceramic tape-casting and simultaneously positive and negative patterning is possible. The ceramic tapes can be easily and fast prepared with a minimal tape thickness of < 400 μm being fully flexible in the gelled state. This flexibility of the gelled ceramic bodies allows complex bending of the tapes in every desired, customizable shape. Complex patterns with a large topological profile from the micrometer range (> 1 μm) down to the sub-micrometer range (≈ 400 nm) and constant aspect ratios over the whole processing route (after gelling and drying and after final sintering) are possible and this makes the ceramic patterning technique a promising alternative to other conventional methods (e.g. embossing, soft-lithography). Furthermore the gel-casting process allows the tailored deposition of a few ceramic particles, which enables the fabrication of patterns with heights below 1 μm . In summary the presented gel-casting process combines the advantages of applying both positive and negative patterns, the pattern accuracy of soft-molding techniques and the possibility of the fabrication of large patterning areas common embossing procedures. The prepared ceramic tapes with controllable micro- and sub-micropatterns are promising candidates for a broad field of applications, e.g. tube inlays with antifouling or drag reduction or interlocking structures.

Acknowledgment

We thank the European Research Council for financial support within the BiocerEng, Project No. 205509.

Appendix A. Supplementary material

Supplementary data associated with this article can be found in the online version at <http://dx.doi.org/10.1016/j.ceramint.2015.12.015>.

References

- [1] Y.T. Liu, T.M. Lee, T.S. Lui, Enhanced osteoblastic cell response on zirconia by bio-inspired surface modification, *Colloids Surf. B-Biointerfaces* 106 (2013) 37–45.
- [2] X. Zhang, et al., Surface functionalization of bioactive glasses with natural molecules of biological significance, Part I: gallic acid as model molecule, *Appl. Surf. Sci.* 287 (2013) 329–340.
- [3] V.C. Ruschel, H.P. Maia, G.C. Lopes, Influence of external and internal surface roughness modifications on ceramic flexural strength, *J. Prosthet. Dent.* 112 (4) (2014) 903–908.
- [4] R. Danzer, On the relationship between ceramic strength and the requirements for mechanical design, *J. Eur. Ceram. Soc.* 34 (15) (2014) 3435–3460.
- [5] D. Lin, et al., Dielectric gradient metasurface optical elements, *Science* 345 (6194) (2014) 298–302.
- [6] F.J.G. de Abajo, Colloquium: Light scattering by particle and hole arrays, *Rev. Mod. Phys.* 79 (4) (2007) 1267–1290.
- [7] Fd.C. Vasconcellos, et al., Printable surface holograms via laser ablation, *ACS Photon* 1 (6) (2014) 489–495.
- [8] D. Nadeem, et al., Embossing of micropatterned ceramics and their cellular response, *J. Biomed. Mater. Res. Part A* 101 (11) (2013) 3247–3255.
- [9] L. Treccani, et al., Antibacterial and abrasion-resistant alumina micropatterns, *Adv. Eng. Mater.* 11 (7) (2009) B61–B66.
- [10] H.A. Abdulbari, et al., Going against the flow—A review of non-additive means of drag reduction, *J. Ind. Eng. Chem.* 19 (1) (2013) 27–36.
- [11] J. Jimenez, Turbulent flows over rough walls, *Annu. Rev. Fluid Mech.* 36 (2004) 173–196.
- [12] E. Zapata-Solvas, et al., Effect of La₂O₃ addition on long-term oxidation kinetics of ZrB₂-SiC and HfB₂-SiC ultra-high temperature ceramics, *J. Eur. Ceram. Soc.* 34 (15) (2014) 3535–3548.
- [13] F. Li, et al., Thermal stability and oxidation resistance of BiCuSeO based thermoelectric ceramics, *J. Alloy. Compd.* 614 (2014) 394–400.
- [14] Y. Liu, et al., Structure, sinterability, chemical stability and conductivity of proton-conducting BaZr_{0.6}Mo_{0.2}Y_{0.2}O_{3-δ} electrolyte membranes: the effect of the M dopant, *J. Membr. Sci.* 467 (2014) 100–108.
- [15] C.L. Diao, et al., Structure, photoluminescence and electrical properties of BaBi₃Eu-5(0).5Ti₄O₁₅ ceramics, *Ceram. Int.* 40 (9) (2014) 13827–13832.
- [16] R.O.A. Souza, et al., Air-particle abrasion on zirconia ceramic using different protocols: Effects on biaxial flexural strength after cyclic loading, phase transformation and surface topography, *J. Mech. Behav. Biomed. Mater.* 26 (2013) 155–163.
- [17] V.V.A. Thampi, et al., Hydroxyapatite, alumina/zirconia, and nanobioactive glass cement for tooth-restoring applications, *Ceram. Int.* 40 (9) (2014) 14355–14365.
- [18] M. Stefanic, et al., Synthesis of bioactive beta-TCP coatings with tailored physico-chemical properties on zirconia bioceramics, *J. Mater. Sci.-Mater. Med.* 25 (10) (2014) 2333–2345.
- [19] E. Bernardo, et al., Novel akermanite-based bioceramics from preceramic polymers and oxide fillers, *Ceram. Int.* 40 (1) (2014) 1029–1035.
- [20] T. Roy, et al., Fabrication and characterization of micro-dimple array on Al₂O₃ surfaces by using a micro-tooling, *Ceram. Int.* 40 (1, Part B) (2014) 2381–2388.
- [21] Mg Holthaus, et al., Micromachining of ceramic surfaces: hydroxyapatite and zirconia, *J. Mater. Process. Technol.* 212 (3) (2012) 614–624.
- [22] A. Hozumi, D.F. Cheng, Facile micropatterning of mesoporous titania film by low-energy electron beam irradiation, *Mater. Chem. Phys.* 129 (1–2) (2011) 464–470.
- [23] J. Berger, et al., Ultraviolet laser interference patterning of hydroxyapatite surfaces, *Appl. Surf. Sci.* 257 (7) (2011) 3081–3087.
- [24] N. Ohashi, et al., Fabrication of ZnO microstructures by anisotropic wet-chemical etching, *J. Electrochem. Soc.* 154 (2) (2007) D82–D87.
- [25] B. Chen, K. Lu, K. Ramsburg, ZnO submicrometer rod array by soft lithographic micromolding with high solid loading nanoparticle suspension, *J. Am. Ceram. Soc.* 96 (1) (2013) 73–79.
- [26] M.G. Holthaus, et al., Versatile crack-free ceramic micropatterns made by a modified molding technique, *J. Am. Ceram. Soc.* 93 (9) (2010) 2574–2578.
- [27] J.A. Lewis, Colloidal processing of ceramics, *J. Am. Ceram. Soc.* 83 (10) (2000) 2341–2359.
- [28] X. Shan, et al., A micro roller embossing process for structuring large-area substrates of laminated ceramic green tapes, *Microsyst. Technol.* 15 (8) (2009) 1319–1325.
- [29] Z.-P. Xie, et al., A new gel casting of ceramics by reaction of sodium alginate and calcium iodate at increased temperatures, *J. Mater. Sci. Lett.* 20 (13) (2001) 1255–1257.
- [30] C. Brandes, et al., Gel casting of free-shapeable ceramic membranes with adjustable pore size for ultra- and microfiltration, *J. Am. Ceram. Soc.* 97 (5) (2014) 1393–1401.
- [31] S. Bertazzo, K. Rezwani, Control of α -alumina surface charge with carboxylic acids, *Langmuir* 26 (5) (2010) 3364–3371.
- [32] Geometrical Product Specifications—Surface texture: Profile method—Terms, definitions and surface texture parameters, in DIN EN ISO 4287, 2010.
- [33] D. Hotza, P. Greil, Review: aqueous tape casting of ceramic powders, *Mater. Sci. Eng.: A* 202 (1–2) (1995) 206–217.
- [34] I. Santacruz, et al., Application of alginate gelation to aqueous tape casting technology, *Mater. Res. Bull.* 37 (4) (2002) 671–682.
- [35] M.I. Nieto, I. Santacruz, R. Moreno, Shaping of dense advanced ceramics and coatings by gelation of polysaccharides, *Adv. Eng. Mater.* 16 (6) (2014) 637–654.
- [36] A. Kristofferson, E. Carlström, Tape casting of alumina in water with an acrylic latex binder, *J. Eur. Ceram. Soc.* 17 (2–3) (1997) 289–297.
- [37] K.Y. Lee, D.J. Mooney, Alginate: properties and biomedical applications, *Prog. Polym. Sci.* 37 (1) (2012) 106–126.
- [38] X. Wang, et al., Gelcasting of silicon carbide based on gelation of sodium alginate, *Ceram. Int.* 28 (8) (2002) 865–871.
- [39] A. Selimovic, et al., Microfluidic device with tunable post arrays and integrated electrodes for studying cellular release, *Analyst* 139 (22) (2014) 5686–5694.
- [40] R. Jagdheesh, Fabrication of a superhydrophobic Al₂O₃ surface using picosecond laser pulses, *Langmuir* 30 (40) (2014) 12067–12073.
- [41] S.K. Donthu, et al., Near-field scanning optical microscopy of ZnO nanopatterns fabricated by micromolding in capillaries, *J. Appl. Phys.* 98 (2) (2005) 024304.
- [42] B. Su, D. Zhang, T.W. Button, Embossing of ceramic micro-pillar arrays, *J. Eur. Ceram. Soc.* 32 (12) (2012) 3345–3349.
- [43] B. Su, D. Zhang, T.W. Button, Micropatterning of fine scale ceramic structures, *J. Mater. Sci.* 37 (15) (2002) 3123–3126.
- [44] M.G. Holthaus, L. Treccani, K. Rezwani, Comparison of micropatterning methods for ceramic surfaces, *J. Eur. Ceram. Soc.* 31 (15) (2011) 2809–2817.
- [45] H.J. Ritzhaupt-Kleissl, et al., Further Ceramic Replication Techniques, in *Microengineering of Metals and Ceramics*, Wiley-VCH Verlag GmbH, Germany, 2008, p. 421–447.